

## Finite Element Simulations of Four-holes Indirect Extrusion Processes of Seamless Tube

Dyi-Cheng Chen<sup>1</sup> and Syuan-Yi Syong<sup>1</sup>

**Abstract:** Finite element simulations are performed to investigate the plastic deformation behavior of Ti-6Al-4V titanium alloy during its indirect extrusion through a four-hole die. The simulations assume the die, mandrel and container to be rigid bodies and ignore the temperature change induced during the extrusion process. Under various extrusion conditions, the present numerical analysis investigates the effective stress and profile of product at the exit. The relative influences of the friction factors, the temperature of billet and the eccentricity of four-hole displacement are systematically examined. The simulations focus specifically on the effects of the friction factor, billet temperature and eccentricity ratio of the four-hole die on the maximum load and effective stress induced within the billet and the taper angle of the extruded tubes. The simulation results provide a useful insight into the optimal processing conditions for the four-hole indirect extrusion of seamless titanium alloy tubes.

**Keywords:** Finite element, indirect extrusion, seamless titanium alloy tubes.

### 1 Introduction

The quality and mechanical properties of indirect-extruded products are directly related to the sectional profile of the die and the processing conditions applied. Lee, Kim and Kang (2005) presented 3D FEM simulations of the porthole die extrusion process used to fabricate the condenser tubes in automobile cooling systems. Ulysse and Johnson (1998) conducted plane-strain upper-bound analyses to evaluate the effect of the process variables in the eccentric single-hole extrusion and unsymmetrical multi-hole extrusion processes, respectively. Ulysse (1999, 2002) combined finite-element analyses with a mathematical programming technique to optimize the design of a two-hole extrusion die and to generate an optimal die flow corrector for flat-faced aluminum extrusion dies, respectively. Peng and Sheppard

---

<sup>1</sup> Department of Industrial Education and Technology, National Changhua University of Education, Changhua 500, Taiwan, R.O.C.

(2004) used FORGE3<sup>TM</sup> FEM software to investigate the correlation between the number and distribution of the die holes in a multi-hole extrusion process and the optimal extrusion parameters.

Zhou, Li and Duszczuk (2004) performed numerical simulations to investigate the isothermal extrusion of 7075 aluminum billets using a varying ram speed. Based upon the simulation results obtained from a series of constant ram speed extrusion runs, the authors presented two ram speed profiles for the isothermal extrusion of aluminum billets at temperatures of 480°C and 500°C, respectively. Chanda, Zhou, Kowalski and Duszczuk (1999) performed 3D FEM simulations based on a rigid-viscoplastic formulation to examine the respective effects of the extrusion ratio and ram speed on the temperature evolution within extruded AA6061 aluminum alloy billets. Elisabetta, Luca and Claudio (2007) conducted 3D FEM simulations to optimize the geometry of porthole-dies for the extrusion of aluminum components. Schikorra, Lambers, Donati, Maier, Tomesani and Tekkaya (2008) analyzed the microstructural evolution of extruded AA6060, AA6082 and AA7075 aluminum billets and used the simulation results to construct micro- and macro-scale material models for predicting the grain size development. Toyama, Kinoshita, Kawano, Sato, Hirata, Kaizu and Ikeda (2008) performed 3D rigid-plastic finite element simulations and model experiments to clarify the influence of the slug cross-section in the simultaneous forward-backward extrusion of A1070 aluminum alloy billets. Many papers combine this equivalent inclusion model with the gradient plasticity to obtain a elastic-plastic constitutive equation [Takashima (2007), Sethuraman and Rajesh (2009), Liu (2009), Hagihara (2007), Qian (2008)]. The current author [Chen, Chen and Wun (2008)] employed rigid-plastic finite element DEFORM<sup>TM</sup> 3D software to investigate the plastic deformation behavior of Ti-6Al-4V titanium alloy during its indirect extrusion through a single-hole die in the seamless tube fabrication process.

In the current study, DEFORM<sup>TM</sup> 3D software is used to investigate the plastic deformation of Ti-6Al-4V titanium alloy during its indirect extrusion through a four-hole die. The simulations focus specifically on the effects of the billet temperature, friction factor, and eccentricity ratio of the die on the stress and load induced within the billet and the taper angle of the extruded tubes.

## 2 Basic Rigid-Plastic FEM Equations

The current simulations are based upon the following assumptions: (1) the die, mandrel and container are all rigid bodies; (2) the Ti-6Al-4V titanium alloy billet is a rigid-plastic material; (3) the friction factors between the extrusion billet and the die, mandrel and container remain constant; and (4) the extrusion process takes place under isothermal conditions. The simulations are based on the following

equations:

Equilibrium equation:

$$\sigma_{ij,j} = 0. \quad (1)$$

Compatibility and incompressibility equations:

$$\dot{\epsilon}_{ij} = \frac{1}{2}(u_{i,j} + u_{j,i}), \quad \dot{\epsilon}_v = u_{i,i} = 0 \quad (2)$$

Constitutive equations:

$$\sigma'_{ij} = \frac{2\bar{\sigma}}{3\dot{\epsilon}} \dot{\epsilon}_{ij}, \quad \bar{\sigma} = \sqrt{\frac{3}{2}(\sigma'_{ij}\sigma'_{ij})}, \quad \dot{\epsilon} = \sqrt{\frac{2}{3}(\dot{\epsilon}_{ij}\dot{\epsilon}_{ij})}. \quad (3)$$

Boundary conditions:

$$\sigma_{ij}n_i = F_j \text{ on } S_F, \quad u_i = U_i \text{ on } S_U. \quad (4)$$

In Eqs. (1) ~ (4),  $\sigma_{ij}$  and  $\dot{\epsilon}_{ij}$  are the stress and the strain velocity, respectively,  $\bar{\sigma}$  and  $\dot{\epsilon}$  are the effective stress and the effective strain velocity, respectively,  $F_j$  is the force acting on the boundary surface of  $S_F$ , and  $U_i$  is the deformation velocity at the boundary surface of  $S_U$ .

The weak form of the rigid-plastic FEM formulation can be determined by applying the variational method to Eqs. (1) ~ (4), i.e.

$$\int \left( \frac{2\bar{\sigma}}{3\dot{\epsilon}} \right) \dot{\epsilon}_{ij} \delta \dot{\epsilon}_{ij} dV + \int K \dot{\epsilon}_{kk} \delta \dot{\epsilon}_{ii} dV - \int_{S_F} F_i \delta u_i dS = 0, \quad (5)$$

where  $V$  and  $S$  are the volume and surface area of the material, respectively, and  $K$  is the penalty constant.

Meanwhile, the frictional boundary condition can be expressed in the following vector form:

$$f = -\frac{2}{\pi} mk \tan^{-1} \frac{|V_s|}{u_0} t, \quad (6)$$

where  $m$  is the friction factor,  $k$  is the local flow stress in shear and  $u_0$  is a positive number with a value much smaller than  $|V_s|$ . Additionally,  $V_s$  is the velocity vector of the billet relative to the die and  $t$  is the unit vector in the direction of  $V_s$ .

The FEM simulations performed in this study are based on a flow formulation approach and an updated Lagrangian procedure. The nonlinear equations in the

FE software are solved using a direct iteration method and the Newton-Raphson scheme. In the solution procedure, the direct iteration method is used to generate suitable initial estimates and the Newton-Raphson method is then used to obtain a rapid convergence to the final solution. The iteration procedure continues until the following termination criteria are satisfied: (1) a velocity error norm of  $\|\Delta \mathbf{v}\| / \|\mathbf{v}\| \leq 0.005$ , and (2) a force error norm of  $\|\Delta F\| / \|F\| \leq 0.05$ , where  $\|\mathbf{v}\|$  is  $(\mathbf{v}^T \mathbf{v})^{1/2}$ .

### 3 Simulation Results and Analysis

Figure 1 presents the finite element model of the symmetrical four-hole extrusion die, while Figure 2 illustrates the geometrical profile of the four-hole die. As shown, the die configuration is characterized by the inner radius ( $D_m$ ) and wall thickness ( $t$ ) of the extruded tube and the eccentricity ratio of the die, i.e.  $e = \frac{b}{a+b}$ ,  $a + b = 16$ .

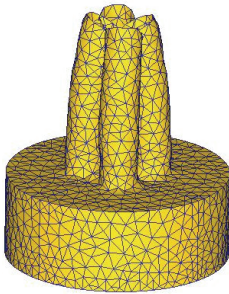


Figure 1: Finite element model of four-hole extrusion process

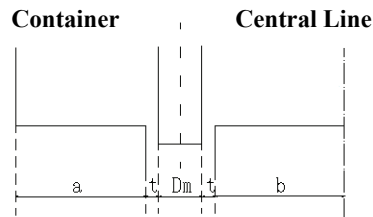
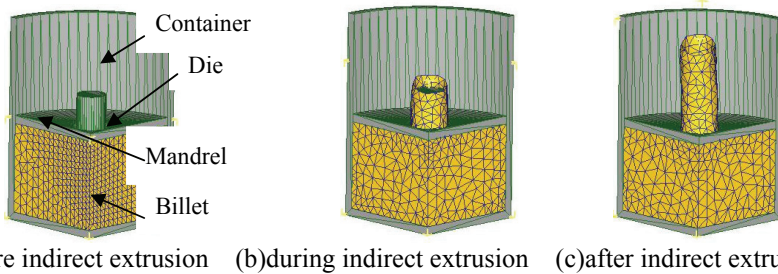


Figure 2: Geometric configuration of four-hole extrusion die

Figure 3 presents mesh models of the billet and die before, during and after the indirect extrusion process. Note that in the simulations, it is assumed that the titanium billet remains firmly attached to the periphery of the mandrel as the die descends, and thus an indirect extrusion of the billet occurs.

Table 1 summarizes the 27 simulation cases considered in the present study. As shown, the simulations utilize three different friction factors, billet temperatures and eccentricity ratio. The rightmost column in the table indicates the maximum load induced in the X-axis direction of the billet during extrusion under the corresponding processing conditions. It is observed that a minimum X-direction load of 2.66 MN is obtained when the extrusion process is performed with a friction factor



(a) before indirect extrusion (b) during indirect extrusion (c) after indirect extrusion  
 Figure 3: Finite element models of titanium alloy billet before, during and after extrusion

of  $m = 0.05$ , a billet temperature of  $T = 850^{\circ}\text{C}$ , and an eccentricity ratio of  $e = 0.7$  (simulation case #9). Moreover, it is apparent that the load induced in the billet reduces with a decreasing friction factor and with an increasing billet temperature or eccentricity ratio.

Figure 4 illustrates the taper angle  $\alpha$  of the extruded product for billets processed at different temperatures. Note that in every case, the friction factor and eccentricity ratio are specified as  $m = 0.05$  and  $e = 0.3$ , respectively. It can be seen that the largest taper angle occurs for a billet temperature of  $T = 750^{\circ}\text{C}$ , while the smallest taper angle occurs for a billet temperature of  $T = 800^{\circ}\text{C}$ .

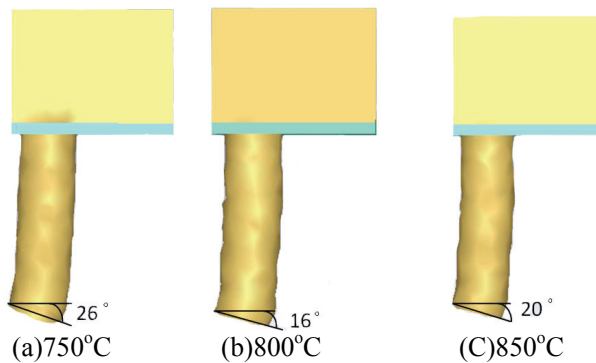


Figure 4: Taper angle  $\alpha$  of extruded product for different billet temperatures ( $m = 0.05$ ,  $e = 0.3$ )

Figure 5 illustrates the variation of the taper angle  $\alpha$  with the value of the friction factor. Note that the simulations assume the temperature and eccentricity ratio to

Table 1: X-load induced in Ti-6Al-4V titanium alloy during four-hole indirect extrusion with different friction factors, billet temperatures, and die eccentricity ratios ( $e = \frac{b}{a+b}$ ,  $a + b = 16$ )

Case No.	m	T°(C)	e	Max. X-load (MN)
Ti-1	0.05	750	0.3	2.84
Ti-2	0.05	750	0.5	2.79
Ti-3	0.05	750	0.7	2.75
Ti-4	0.05	800	0.3	2.83
Ti-5	0.05	800	0.5	2.78
Ti-6	0.05	800	0.7	2.72
Ti-7	0.05	850	0.3	2.83
Ti-8	0.05	850	0.5	2.78
Ti-9	0.05	850	0.7	2.66
Ti-10	0.1	750	0.3	2.99
Ti-11	0.1	750	0.5	2.84
Ti-12	0.1	750	0.7	2.78
Ti-13	0.1	800	0.3	2.97
Ti-14	0.1	800	0.5	2.83
Ti-15	0.1	800	0.7	2.74
Ti-16	0.1	850	0.3	2.94
Ti-17	0.1	850	0.5	2.81
Ti-18	0.1	850	0.7	2.72
Ti-19	0.2	750	0.3	3.10
Ti-20	0.2	750	0.5	2.90
Ti-21	0.2	750	0.7	2.82
Ti-22	0.2	800	0.3	3.09
Ti-23	0.2	800	0.5	2.90
Ti-24	0.2	800	0.7	2.81
Ti-25	0.2	850	0.3	3.08
Ti-26	0.2	850	0.5	2.88
Ti-27	0.2	850	0.7	2.80

be  $T = 750^\circ\text{C}$  and  $e = 0.5$ , respectively, in every case. The results show that the largest taper angle occurs when the friction factor is specified as  $m = 0.05$ , while the smallest taper angle occurs for a friction factor of  $m = 0.2$ . Overall, it is observed that the taper angle of the extruded tubes reduces with an increasing friction factor. Figure 6 shows the effect of the eccentricity ratio on the taper angle  $\alpha$  of the ex-

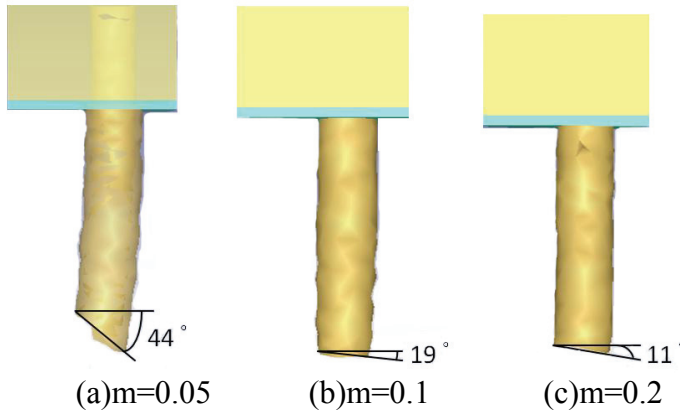


Figure 5: Taper angle  $\alpha$  of extruded product for different friction factors ( $T = 750^{\circ}\text{C}$ ,  $e = 0.5$ )

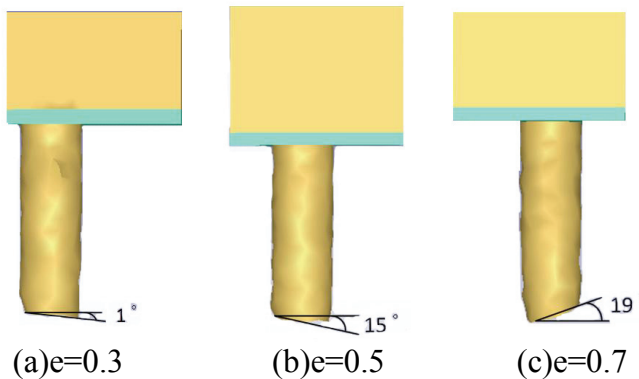


Figure 6: Taper angle  $\alpha$  of extruded product for different eccentricity ratios ( $m = 0.05$ ,  $T = 800^{\circ}\text{C}$ )

truded product for a constant friction factor and billet temperature of  $m = 0.05$  and  $T=800^{\circ}\text{C}$ , respectively. It can be seen that the lowest taper angle occurs for an eccentricity ratio of  $e = 0.3$ , while the largest taper angle occurs for an eccentricity ratio of  $e = 0.7$ . In other words, the taper angle  $\alpha$  of the extruded tube reduces with a decreasing eccentricity ratio.

Figure 7 illustrates the distribution of the effective stress in extruded titanium tubes with inner radii of 7 mm and wall thicknesses of 1 mm following their indirect extrusion using seven different processing designs. It can be seen that the maximum

effective stress occurs in the outer region of the tubes as they exit the die. Furthermore, it is apparent that the effective stress increases with a larger eccentricity ratio (Case Ti-3,  $e=0.7$ ) and a higher friction factor (Cases Ti-10 and Ti-19,  $m=0.1$  and  $m=0.2$ , respectively).

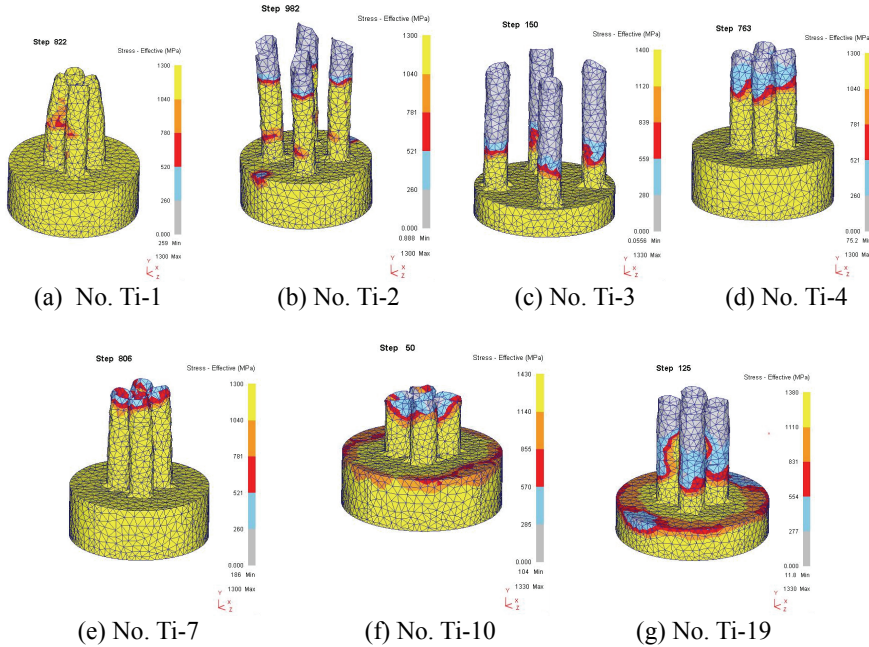


Figure 7: Distribution of effective stress in extruded titanium tube with inner radius of 7 mm and wall thickness of 1 mm following indirect extrusion using different processing designs

#### 4 Conclusions

This study has performed a series of numerical simulations using DEFORM<sup>TM</sup> 3D finite element software to investigate the plastic deformation of Ti-6Al-4V titanium alloy during its indirect extrusion through a four-hole die in the seamless tube fabrication process. The major findings can be summarized as follows:

1. The load induced in the billet reduces with a reducing friction factor and an increasing billet temperature or die eccentricity ratio.

2. The taper angle  $\alpha$  of the extruded tubes reduces with an increasing friction factor or a reducing eccentricity ratio.
3. The effective stress induced in the extruded product increases with an increasing eccentricity ratio or friction factor.

## 5 References

- Chanda, T.; Zhou, J.; Kowalski, L.; Duszczyk, J.** (1999): 3D FEM simulation of the thermal events during AA6061 aluminum extrusion. *Scripta Materialia*, vol. 41, no. 2, pp. 195-202.
- Chen, D. C.; Chen, J. Y.; Wun, K.C.** (2008): Forming design and simulation in indirect extrusion processes of seamless tube. *The 8<sup>th</sup> Asia Pacific Conference on Materials Processing*, Guilin-Guangzhou, China, pp. 951-957.
- Elisabetta, C.; Luca, M.; Claudio, G.** (2007): 3D FEM geometry and material flow optimization of porthole-die extrusion. *AIP Conf. Proc. -Materials Processing and Design: Modeling, Simulation and Applications*, vol. 908, pp. 419-424.
- Hagihara, S.; Tsunori, M.; Ikeda, T.; Miyazaki, N.** (2007): Application of Meshfree method to elastic-plastic fracture mechanics parameter analysis. *CMES: Computer Modeling in Engineering & Sciences*, vol. 17, no. 2, pp. 63-72.
- Lee, J. M.; Kim, B. M.; Kang, C. G.** (2005): Effects of chamber shapes of porthole die on elastic deformation and extrusion process in condenser tube extrusion. *Materials and Design*, vol. 26, pp. 327-336.
- Liu, D. S.; Tsai, C. Y.; Lyu, S. R.** (2009): Determination of temperature-dependent elastio-plastic properties of thin-film by MD nanoindentation simulations and an inverse GA/FEM computational scheme. *CMC: Computers, Materials & Continua*, vol. 11, no. 2, pp. 147-164.
- Peng, Z.; Sheppard, T.** (2004): Simulation of multi-hole die extrusion. *Materials Science and Engineering A*, vol. 367, pp. 329-342.
- Qian, X.; Cao, Y.; Zhang, J.; Raabe, D.; Yao, Z.; Fei, B.** (2008): An inverse approach to determine the mechanical properties of elastoplastic materials using indentation tests. *CMC: Computers, Materials & Continua*, vol. 7, no. 1, pp. 33-41.
- Schikorra, M.; Lambers, H.-G.; Donati, L.; Maier, H. J.; Tomesani, L.; Tekkaya, A. E.** (2008): Microstructure development during extrusion of AA6060, AA6082 and AA7075 alloys. *The 9<sup>th</sup> International Conference on Technology of Plasticity*, Gyeongju, Korea, pp. 1471-1477.
- Toyama, M.; Kinoshita, H.; Kawano, M.; Sato, M.; Hirata, K.; Kaizu, K.;**

**Ikeda, M.** (2008). Influence of slug shape on metal flow in simultaneous forward-backward extrusion of compound gear. *The 9<sup>th</sup> International Conference on Technology of Plasticity*, Gyeongju, Korea, pp. 1561-1566.

**Sethuraman, R.; Rajesh, N. R.** (2009): Evaluation of elastic-plastic crack tip parameters using partition of unity finite element method and pseudo elastic analysis. *CMES: Computer Modeling in Engineering & Sciences*, vol. 39, no. 1, pp. 67-99.

**Takashima, S.; Nakagaki, M.; Miyazaki, N.** (2007): An elastic-plastic constitutive equation taking account of particle size and its application to a homogenized finite element analysis of a composite material. *CMES: Computer Modeling in Engineering & Sciences*, vol. 20, no. 3, pp. 193-202.

**Ulysse, P.; Johnson, R. E.** (1998): A study of the effect of the process variables in unsymmetrical single-hole and multi-hole extrusion processes. *Journal of Materials Processing Technology*, vol. 73, pp. 213-225.

**Ulysse, P.** (1999): Optimal extrusion die design to achieve flow balance. *International Journal of Machine Tools and Manufacture*, vol. 39, pp. 1047-1064.

**Ulysse, P.** (2002): Extrusion die design for flow balance using FE and optimization methods. *International Journal of Mechanical Sciences*, vol. 44, pp. 319-341.

**Zhou, J.; Li, L.; Duszcyk, J.** (2004): Computer simulated and experimentally verified isothermal extrusion of 7075 aluminum through continuous ram speed variation. *Journal of Materials Processing Technology*, vol. 146, pp. 203-212.